


Tunable frequency-bin multimode squeezed vacuum states of lightChristian Drago ^{1,2,*} and Agata M. Brańczyk³¹*Department of Physics and Astronomy, University of Waterloo, 200 University Avenue West, Waterloo, Ontario, Canada N2L 3G1*²*Department of Physics, University of Toronto, 60 St. George Street, Toronto, Ontario, Canada M5S 1A7*³*Perimeter Institute for Theoretical Physics, Waterloo, Ontario, Canada N2L 2Y5*

(Received 13 May 2022; accepted 19 September 2022; published 20 October 2022)

Squeezed states are a versatile class of quantum states with applications ranging from quantum computing to high-precision detection. We propose a method for generating tunable squeezed vacuum states of light with multiple modes encoded in frequency bins. Our method uses custom-engineered spontaneous parametric down-conversion pumped by a pulse-shaped pump field. The multimode squeezed states are generated in a single pass and can be tuned in real time by adjusting the properties of the pump field. Exploring new quantum states of light, encoded in new degrees of freedom, can be a fruitful path toward discovering new quantum applications.

DOI: [10.1103/PhysRevA.106.043714](https://doi.org/10.1103/PhysRevA.106.043714)**I. INTRODUCTION**

Quantum light is a key ingredient in emerging quantum technologies such as quantum communication [1], quantum cryptography [2], quantum computing [3], quantum imaging [4], and quantum metrology [5]. Its broad application results from the wide variety of available degrees of freedom (e.g., polarization, frequency, and temporal mode), which in turn can encode a wide variety of quantum states (e.g., qubits, Fock states, and cat states). Exploring the generation of new quantum states, with unique sets of properties, can lead to the development of new quantum technologies.

A versatile class of quantum states are known as squeezed vacuum states [6] or simply squeezed states. (For a brief review of squeezed vacuum states, refer to Appendix A.) They are typically classified by the number of modes they populate, where different kinds of squeezed states are better suited for different applications. Single-mode squeezed states have reduced quantum noise in one degree of freedom, making them most useful for quantum cryptography [2] and quantum metrology [5]. Two-mode squeezed states, on the other hand, possess entanglement between the modes of the electromagnetic field and can be used for quantum teleportation [1]. Squeezed states can also be distributed across multiple modes. These multimode squeezed states can be used to generalize various quantum information protocols, e.g., multiparameter quantum metrology [7], multichannel quantum imaging [8], and multipartite teleportation [9], or be used for quantum computation [10].

The generalization of single- and two-mode squeezed states was first proposed by Yuen [11] and later by Yeoman and Barnett [12]. Yeoman and Barnett considered states that had both single- and two-mode squeezing properties and proposed a method to generate them with two single-mode squeezed states and a beam splitter. This method was

generalized to include multimode squeezed states by van Loock and Braunstein [13], who proposed using a sequence of N beam splitters to prepare a multimode squeezed state entangled across N spatial modes. This method requires interferometric stabilization of the optical paths and indistinguishability between frequency and polarization modes [14]. To overcome these challenges, another approach was proposed [15,16] in which an optical parametric oscillator (OPO) and a single periodically poled ferroelectric crystal is used to generate N -mode entangled states between the cavity modes of the OPO. This method was further expanded upon by multiplexing the light in time, allowing an unlimited number of entangled modes [17,18]. Further, one can encode squeezed state modes into Schmidt modes [19]. These newer methods are much more compact and stable and benefit from the intrinsic compatibility of frequency and time encodings with waveguides and fiber transmission, and we expand on them here.

We introduce a method for generating tunable multimode squeezed states of light encoded in frequency bins. Our proposal builds on the idea that frequency-bin entanglement can be generated by domain-engineered down-conversion, which was recently demonstrated by Morrison *et al.* [20]. We show how the addition of a frequency-shaped pump can yield grid states similar to the two-photon joint spectral amplitudes introduced by Fabre *et al.* [10], but with more control over the peaks and without the need for a cavity (at the expense of fewer modes available). We further show how, with the addition of frequency filtering, one can create a squeezed state that can be tuned from a single mode to two modes in real time.

Our method for generating multimode squeezed states differs from previous proposals in several ways: (i) Unlike [10,15–18], our method does not require a cavity to generate multiple modes; (ii) unlike [12,13], our method does not require increasingly more beam splitters to generate more modes; and (iii) unlike the Schmidt modes [19], which are difficult to distinguish experimentally due to their complex

*christian.drago@mail.utoronto.ca

spectral shape, our modes are encoded in discrete frequency bins and can be distinguished by their central frequencies. Furthermore, our method allows the squeezing parameters of the state to be tuned in real time. Depending on the application, these properties may make this method advantageous over other methods.

II. FREQUENCY BIN ENCODING

A desirable property of quantum light is localization in space and time, which makes it possible to deliver wave packets of quantum light in a clocked manner [21]. A Gaussian-like frequency encoding satisfies these properties. As with their cw counterparts [15,16], such an encoding is intrinsically compatible with waveguides and fiber transmission.

To encode our modes we define a multifrequency field operator from the usual bosonic field operator $\hat{a}(\omega)$ by

$$\hat{A}_n = \int d\omega G_n(\omega)\hat{a}(\omega), \quad (1)$$

where $\{G_n(\omega)\}$ describe nonoverlapping Gaussian-like pulses such that to good approximation

$$\int d\omega G_n(\omega)G_m(\omega) = \delta_{nm} \quad (2)$$

and thus

$$[\hat{A}_n, \hat{A}_m^\dagger] = \delta_{nm}. \quad (3)$$

In terms of these operators, the multimode squeezed state takes the form

$$|\psi\rangle = \exp\left(\frac{1}{2} \sum_{n,m} \gamma_{nm} \hat{A}_n^\dagger \hat{A}_m^\dagger - \text{H.c.}\right) |\text{vac}\rangle, \quad (4)$$

which can be rewritten as

$$|\psi\rangle = \exp\left(\frac{1}{2} \int d\omega_i d\omega_s h(\omega_s, \omega_i) \hat{a}^\dagger(\omega_i) \hat{a}^\dagger(\omega_s) - \text{H.c.}\right) |\text{vac}\rangle, \quad (5)$$

if $h(\omega_s, \omega_i)$ can be decomposed as

$$h(\omega_s, \omega_i) = \sum_{n,m} \gamma_{nm} G_n(\omega_i) G_m(\omega_s), \quad (6)$$

where γ_{nm} is in general complex and taken to be symmetric. The decomposition in Eq. (6) cannot be general because a set of Gaussian functions are not exactly orthogonal nor are they complete. However, for the $h(\omega_s, \omega_i)$ we consider, the decomposition in Eq. (6) is exact. The state in Eq. (5) could in principle be generated by type-I spontaneous parametric down-conversion (where both idler and signal modes have the same polarization) if one had means of engineering a joint spectral amplitude of the form given by (6). To date, most joint-spectral engineering methods have been developed for type-II parametric down-conversion (where both idler and signal have orthogonal polarization), so we will focus on a type-II setup in this paper. In the next section we show how to use spectrally engineered type-II down-conversion to generate a state that, once sent through a Mach-Zehnder interferometer with a half waveplate (HWP) set to 45° in one arm, is equal to the multimode squeezed state in (4).

III. IMPLEMENTATION WITH SPONTANEOUS PARAMETRIC DOWN-CONVERSION

We consider type-II spontaneous parametric down-conversion [22] under the following conditions: (i) rotating-wave approximation, (ii) undepleted pump approximation, (iii) ignoring time-ordering effects, (iv) symmetric group-velocity matching, and (v) linear phase mismatch (see Appendix B for a discussion of the assumptions). In this regime, the state generated by this process is

$$|\psi\rangle = \exp\left(i\gamma \int d\omega_i d\omega_s f(\omega_s, \omega_i) \hat{a}_H^\dagger(\omega_i) \hat{a}_V^\dagger(\omega_s) - \text{H.c.}\right) \times |\text{vac}\rangle, \quad (7)$$

where γ is the squeezing parameter and

$$f(\omega_s, \omega_i) = \alpha(\omega_s + \omega_i) \phi(\omega_s - \omega_i) \quad (8)$$

is the joint spectral amplitude (JSA). The JSA is given by the spectral profile of the pump $\alpha(\omega_s + \omega_i)$ and the normalized phase-matching function $\phi(\omega_s - \omega_i)$ which depends on the properties of the nonlinear material. Following the normalization of the pump and phase-matching function in Appendix B, the joint spectral amplitude is normalized according to

$$\int d\omega_s d\omega_i |f(\omega_s, \omega_i)|^2 = 1. \quad (9)$$

A. Designing the joint spectral amplitude

Our goal is to design the pump-envelope function $\alpha(\omega_s + \omega_i)$ and the phase-matching function $\phi(\omega_s - \omega_i)$ such that the joint spectral amplitude $f(\omega_s, \omega_i)$ in Eq. (8) matches the target joint spectral amplitude $h(\omega_s, \omega_i)$ in Eq. (6). To achieve this, the pump envelope function should be prepared as a superposition of Gaussian-like functions centered at different frequencies

$$\alpha(\omega_s + \omega_i) = \sum_{n=-N}^N \frac{a_n}{(4\pi\sigma^2)^{1/4}} e^{-(\omega_s + \omega_i - \Omega_p + n\delta\omega)^2/8\sigma^2} \quad (10)$$

for some set of dimensionless constants a_n and integers n . The pump envelope function can be customized with various pulse-shaping techniques (for a review of pulse shaping in various regimes see [23–25]). Since the pump function is square normalized, the coefficients satisfy $\sum_n a_n^2 = 1$.

The phase-matching function should also be a superposition of Gaussian-like functions, centered at different frequencies

$$\phi(\omega_s - \omega_i) = \sum_{m=-N}^N \frac{b_m}{(4\pi\sigma^2)^{1/4}} e^{-[\omega_s - \omega_i - (\Omega_s - \Omega_i) - m\delta\omega]^2/8\sigma^2}, \quad (11)$$

where b_m are some set of dimensionless amplitude coefficients that satisfy $\sum_m b_m^2 = 1$ and m is an integer. We will show how to customize the phase-matching function using customizing in Sec. III B. In the meantime, we note that if the widths of each term in the phase-matching function (PMF) and pump are the same and we insert Eqs. (10) and (11) into Eq. (8), we

yield the joint spectral amplitude

$$f(\omega_s, \omega_i) = \frac{1}{\sqrt{2}} \sum_{n,m} a_{n-m} b_{n+m} G_n(\omega_s) G_m(\omega_i), \quad (12)$$

where for the remainder of this section the summations are over n and m such that $n - m = \pm 1, \pm 2, \dots, \pm N$ and

$$G_n(\omega_J) = \frac{e^{-(\omega_J - \Omega_J - \Omega_n)^2/4\sigma^2}}{(2\pi\sigma^2)^{1/4}}, \quad (13)$$

where $\Omega_n \equiv n\delta\omega/2$ and $J = s, i$ runs over the two signal and idler frequencies. When absolute value squared, these functions yield Gaussian intensity distributions, which are optimal for such decompositions [26]. Finally, if $|\Omega_n - \Omega_m| \gg \sigma$, then to good approximation $G_n(\omega)$ satisfies the orthogonality condition given by Eq. (2).

Inserting the decomposition of the JSA in Eq. (12) into the down-converted state in Eq. (7), defining $\gamma_{nm} \equiv \gamma a_{n-m} b_{n+m} / \sqrt{2}$, and using the definition of the mode A_n in Eq. (1) yields

$$|\psi\rangle = \exp\left(\sum_{n,m} \gamma_{nm} \hat{A}_{n,H}^\dagger \hat{A}_{m,V}^\dagger - \text{H.c.}\right) |\text{vac}\rangle. \quad (14)$$

This a multimode squeezed state in the Gaussian-mode degree of freedom and a two-mode squeezed state in the polarization degree of freedom (indicated by the subscripts H and V). To eliminate the polarization degree of freedom, we pass the state through a Mach-Zehnder interferometer with a HWP set to 45° in one arm. The output state is

$$|\psi'\rangle = \bigotimes_{j=1,2} \exp\left(\frac{(-1)^j}{2} \sum_{n,m} \gamma_{nm} \hat{A}_{n,j}^\dagger \hat{A}_{m,j}^\dagger - \text{H.c.}\right) |\text{vac}\rangle, \quad (15)$$

which consists of two copies of a multimode squeezed state, all in the same polarization, where the subscript $j = 1, 2$ labels the output modes of the interferometer.

B. Customizing the phase-matching function

We now turn to designing an appropriately shaped phase-matching function. Consider a nonlinear material whose nonlinearity can vary along the longitudinal direction z ; this variation can be captured by a dimensionless function $g(z)$ [defined in Eq. (B3)]. The function $g(z)$ can be transformed as

$$\Phi(\Delta k(\omega_s, \omega_i)) = \frac{1}{L} \int_{-L/2}^{L/2} dz g(z) e^{i\Delta k(\omega_s, \omega_i)z}, \quad (16)$$

which we can think of as an unnormalized phase-matching function. Here L is the length of the nonlinear material and $\Delta k(\omega_s, \omega_i) = k_p(\omega_s + \omega_i) - k_i(\omega_i) - k_s(\omega_s)$ is the phase mismatch, where $k_J(\omega_J) = \omega_J n_J(\omega_J)/c$, with $n_J(\omega_J)$ the refractive index for the mode J , c the speed of light, and $J = s, i$. The unnormalized phase-matching function $\Phi(\Delta k(\omega_s, \omega_i))$ is related to the normalized phase-matching function $\phi(\omega_s - \omega_i)$ via Eq. (B16). When modeling custom-poled materials, it is easier to work with the unnormalized function $\Phi(\Delta k(\omega_s, \omega_i))$ and then to normalize the function numerically at the end.

The target phase-matching function can then be written, in unnormalized form, as

$$\Phi(\Delta k) = \sum_{m=-N}^N c_m e^{-(\Delta k - \Delta k_0 - m\delta k)^2/8\sigma_k^2}, \quad (17)$$

where

$$\sigma_k = \frac{\sigma}{2}(k'_s - k'_i), \quad (18)$$

$$\delta k = \frac{\delta\omega}{2}(k'_s - k'_i), \quad (19)$$

and together with the Taylor expansion of $\Delta k(\omega_s, \omega_i)$ in Eq. (B14) is equivalent to Eq. (11).

To generate the desired phase-matching function, we must determine the right form of $g(z)$. In principle, one can imagine varying $g(z)$ continuously. Such methods, however, do not exist for nonlinear crystals; in practice, for a given crystal, $g(z)$ is constrained to take on values of ± 1 [27]. Experimentally, the sign of $g(z)$ can be alternated using a technique known as ferroelectric poling [28–31], giving rise to individual domains. In Δk space, each crystal domain contributes a sinc function with a phase that depends on the domain position and orientation. By carefully arranging the positive and negative domains in $g(z)$, it is possible to interfere the sinc functions to construct phase-matching functions with almost arbitrary shapes. As with all quasi-phase-matching techniques, such as periodic poling, the resulting amplitude will necessarily be reduced when compared with intrinsically phase-matched materials.

Several methods for designing appropriate domain configurations have been developed [32–40]. Here we focus on a variation of the algorithm originally proposed in [37] and further developed in [40,41] (effects of experimental imperfections in this approach were examined by Fejer *et al.* [29] and recently by Graffitti *et al.* [42]). In this approach, one computes an amplitude function, defined as the PMF, evaluated at a specific value of Δk , along the length of the crystal, and then selects domains (one at a time from left to right) that bring the customized crystal's amplitude function closer to the target amplitude function. When the customized crystal's amplitude function closely approximates the target amplitude function at all points within the crystal, the customized crystal's PMF will also closely approximate the target PMF. This approach was recently demonstrated for an eight-peak PMF in potassium titanyl phosphate (KTP) [20].

In Appendix D we derive the following constraint on c_m :

$$c_0 + 2 \sum_{m=1}^N c_m \leq \sqrt{\frac{2}{\pi}} \frac{1}{L\sigma_k}. \quad (20)$$

For the simple case where c_m are all equal, the condition reduces to

$$c_m = \sqrt{\frac{2}{\pi}} \frac{1}{L\sigma_k N_G}, \quad -N \leq m \leq N, \quad (21)$$

where N_G is the number of Gaussian amplitudes. It is desirable to maximize the conversion efficiency and thus to maximize c_m within these constraints.

Our implementation of the algorithm uses domain widths equal to the crystal's coherence length. As a result, the

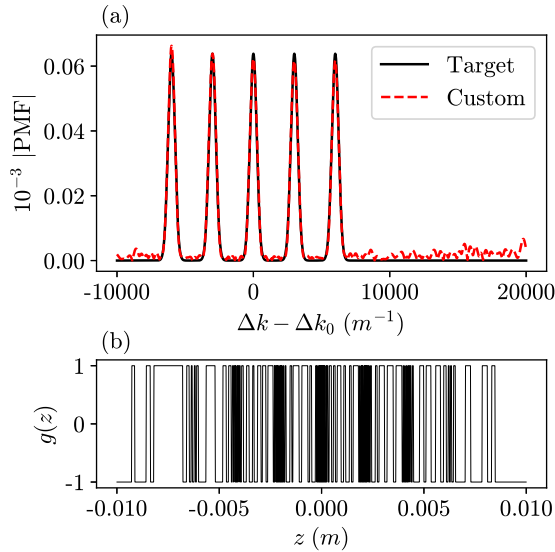


FIG. 1. (a) Five-peak target phase-matching function as defined in Eq. (17) (with $c_m = \sqrt{2}/\sqrt{\pi}L\sigma_k 5$, $\sigma_k = 2.5/L$, and $\delta k = 24\sigma_k$) and corresponding custom phase-matching function generated by the custom-poled crystal shown in (b). We took $\sigma_k = 2.5/L$ to ensure that the target nonlinearity profile fits within the length of the crystal. The custom-poled crystal has $N = 1073$ domains of width $w = 18.63 \mu\text{m}$. The domain width was chosen to match the phase-matching conditions of type-II KTP in the symmetric group-velocity-matched regime.

phase-matching function is constrained to be real and the coefficients should satisfy $c_m \approx c_{-m}$ (the approximation in this equality comes from a slight bias in the PMF discussed in Appendix C). These restrictions would be lifted if a sub-coherence-length version of the algorithm was implemented [40]. In the next section we demonstrate how to apply this technique to a specific example.

IV. EXAMPLE: 15-MODE SQUEEZED STATES

As an example, we customize a 2-cm KTP crystal to generate a PMF with five Gaussian peaks centered at $\Delta k_0 - m\delta k$, where $m = (0, \pm 1, \pm 2)$ and $\delta k = 24\sigma_k$. We set $\sigma_k = 2.5/L$ to ensure that the target nonlinearity profile fits within the length of the crystal. The target PMF is given by Eq. (17) with $N = 2$. Figure 1 shows the generated PMF compared to the target PMF, as well as the resulting domain configuration $g(z)$. Notice the expected slight bias in the generated PMF discussed in Appendix C.

We design a pump function with five peaks centered at $\omega = \Omega_p - n\delta\omega$, where $n = (0, \pm 1, \pm 2)$. As with the PMF, we take all coefficients c_m to be real, equal, and given by the restriction in Eq. (21). We take $\sigma = 2\sigma_k/(k'_p - k'_s)$, and to ensure that the spacing is the same as for the PMF we take $\delta\omega = 24\sigma$. Then using Eq. (18) and $\sigma_k = 2.5/L$, the pump bandwidth in frequency is $\sigma/2\pi = 0.127 \text{ THz}$ and in time is on the order of 7 ps. The resulting JSA with corresponding PMF and pump is shown in Fig. 2. Each peak in the JSA corresponds to a term in Eq. (14). Notice that there is a slight bend in the PMF due to dispersion (for these plots, we used the full Sellmeier equations rather than the first-order approximation

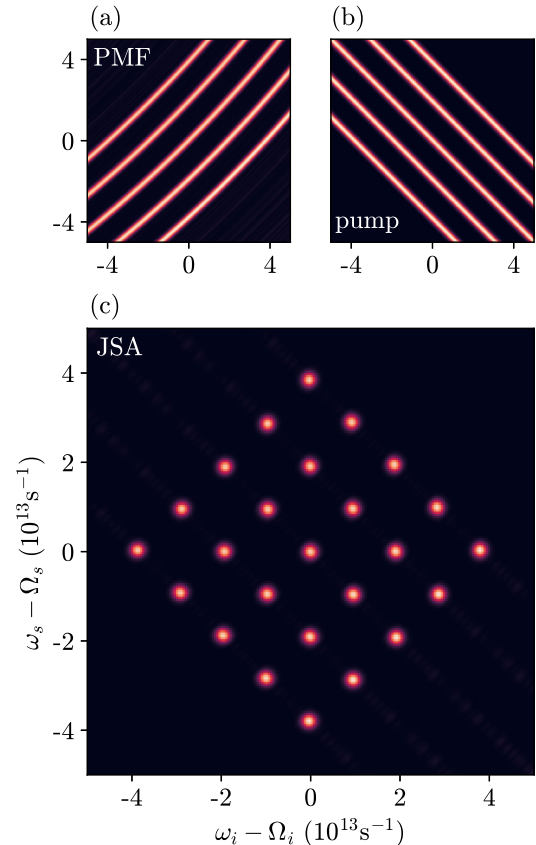


FIG. 2. (a) Five-peak phase-matching function as defined by Eq. (11) with σ and $\delta\omega$ related to σ_k and δk in Fig. 1 via Eqs. (18) and (19). (b) Five-peak pump function as defined in Eq. (10) with the same σ and $\delta\omega$ as the PMF. (c) Resulting joint spectral amplitude as defined in Eq. (8).

of Δk). Too much dispersion will reduce the effectiveness of this technique, but in the example shown here, the effect on the JSA is negligible.

It is possible to tune the amplitudes γ_{nm} to some extent by tuning the height of the peaks in the pump function (the height of the peaks in the PMF are fixed for a given crystal). Tuning the peak of the pump function is equivalent to scaling the height of the modes that lie along the same antidiagonal in the JSA.

The JSA in Fig. 2 has 25 peaks, but it corresponds to a 15-mode squeezed state because the PMF is symmetric in its amplitudes. The JSA is also symmetric along the line $\omega_s = \omega_i$. There are ten amplitudes above the line $\omega_s = \omega_i$ which are all centered at different frequencies and thus correspond to two-mode squeezing terms. Each amplitude along the diagonal is centered at the same center frequency and thus corresponds to each of the five single-mode squeezing terms.

V. EXTENSION: TUNABLE HYBRID SQUEEZED STATES

In this section we introduce and describe the generation of hybrid squeezed states, which have features of single-mode and two-mode squeezed vacuum states. Consider the special case of the multimode squeezed state [Eq. (A3)] restricted to

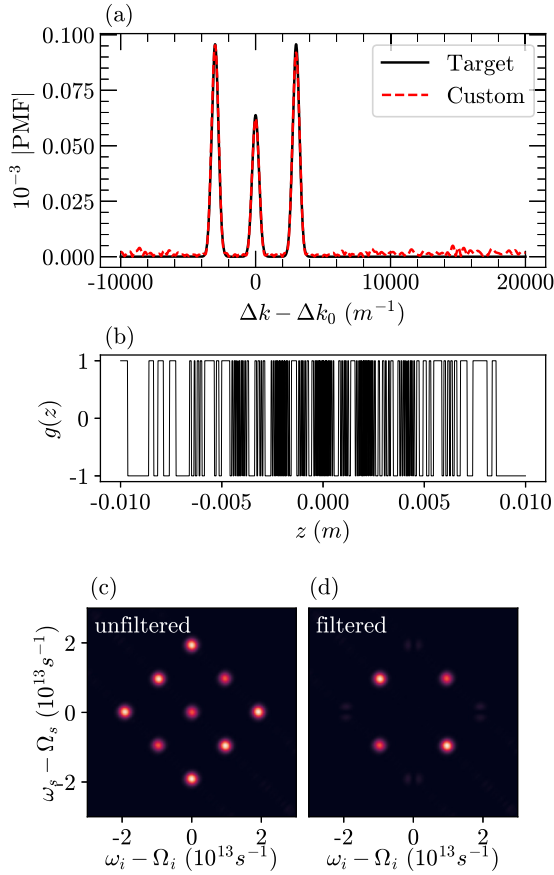


FIG. 3. (a) Three-peak target phase-matching function as defined in Eq. (17) (with $c_0 = \sqrt{2}/\sqrt{\pi}L5\sigma_k$ and $c_1 = c_{-1} = 3c_0/2$) and corresponding custom phase-matching function generated by the custom-poled crystal shown in (b). The parameters σ_k , δk , N , and w are the same as in Fig. 1. (c) Resulting joint spectral amplitude as defined in Eq. (8) for a three-peak phase-matching function and a three-peak pump function with σ and $\delta\omega$ the same as in (a). (d) The JSA in (c) with a filter applied to both the signal and idler modes, with a transmission function $\{1 - \exp[-(\omega_s - \Omega_s)^2/4\sigma_f^2]\} \{1 - \exp[-(\omega_i - \Omega_i)^2/4\sigma_f^2]\}$, where $\sigma_f = 2\sigma$.

two modes

$$|\text{THSS}\rangle = e^{(\beta_{11}/2)\hat{a}_1^\dagger\hat{a}_1^\dagger + \beta_{12}\hat{a}_1^\dagger\hat{a}_2^\dagger + (\beta_{22}/2)\hat{a}_2^\dagger\hat{a}_2^\dagger - \text{H.c.}} |\text{vac}\rangle, \quad (22)$$

where we restricted $\beta_{12} = \beta_{21}$. We can tune the constants to continuously move between a single-mode squeezed state ($\beta_{12} = \beta_{22} = 0$), a two-mode squeezed state ($\beta_{11} = \beta_{22} = 0$), or a product of two single-mode squeezed states ($\beta_{12} = 0$). We call this a tunable hybrid squeezed state (THSS).

Using the pulse-mode encoding introduced in Sec. II, a JSA corresponding to a THSS has four amplitudes located at, say, $(\Omega_{-1}, \Omega_{-1})$, (Ω_{-1}, Ω_1) , (Ω_1, Ω_{-1}) , and (Ω_1, Ω_1) , each corresponding to a squeezing term in Eq. (22). To generate such a JSA, we create a three-peak PMF and a three-peak pump function, to produce a nine-peak JSA show in Fig. 3. The JSA in Fig. 3 has extra squeezing terms located at Ω_0 . However, the full state generated from the JSA in Fig. 3 can be written as a product of two squeezing operators acting on

the vacuum state given by

$$|\psi\rangle = \left[\exp\left(\frac{\gamma_{11}}{2}\hat{A}_1^\dagger\hat{A}_1^\dagger + \frac{\gamma_{-11}}{2}\hat{A}_{-1}^\dagger\hat{A}_1^\dagger + \frac{\gamma_{-1-1}}{2}\hat{A}_{-1}^\dagger\hat{A}_{-1}^\dagger - \text{H.c.}\right) \right] \times \left[\exp\left(\gamma_{-20}\hat{A}_{-2}^\dagger\hat{A}_0^\dagger + \frac{\gamma_{00}}{2}\hat{A}_0^\dagger\hat{A}_0^\dagger + \gamma_{20}\hat{A}_2^\dagger\hat{A}_0^\dagger - \text{H.c.}\right) \right] |\text{vac}\rangle. \quad (23)$$

We can always decompose the state in this way because the modes are orthogonal and thus $[A_n, A_m^\dagger] = \delta_{nm}$. This is crucial because it means the state corresponding to Fig. 3 can be written as $|\psi\rangle = |\text{THSS}\rangle \otimes |\phi\rangle$ and thus $|\phi\rangle$ can be traced out without degrading the purity of the desired modes. To trace out the state $|\phi\rangle$ in practice, we can pass the nine-peak JSA state through a spectral filter that blocks frequencies around Ω_0 . The resulting JSA is shown in Fig. 3(d).

This hybrid squeezed state can be tuned in real time by tuning the amplitude of each term in the pump function. This is because each term in the pump function uniquely corresponds to terms in the squeezing operator; specifically, each peak centered at (Ω_n, Ω_m) corresponds to the squeezing term associated with the $A_n A_m$ operators in (23). The middle peak in the pump amplitude generates two JSA amplitudes at (Ω_{-1}, Ω_1) and (Ω_1, Ω_{-1}) , but these both contribute to the same amplitude in the squeezed state. Since the pump is a function of three center frequencies with no overlap we can independently vary the amplitude of all three and thus tune the squeezing parameters of the final squeezed state independently.

VI. CONCLUSION

We have proposed a method for generating multimode squeezed states of light encoded in Gaussian-like frequency modes. This method differs from related methods [10,12,13,15–19] in several ways that might make it advantageous, depending on the application.

The proposed method relies on customizing the joint spectral properties of light generated via spontaneous parametric down-conversion, which requires two independent ingredients. The first is the spectral engineering of light incident on the crystal, which we took as a given. The second is the engineering of the nonlinear crystal to have desired phase-matching properties (captured by the phase-matching function), for which we used an algorithm [40] that takes as an input the target phase-matching function and outputs a binary string that defines poles in a ferroelectrically poled crystal [43].

We used this method to design two kinds of squeezed vacuum states. The first is an N -mode squeezed vacuum state, which could generalize various quantum information protocols [7–9]. The second is a tuneable hybrid squeezed vacuum state, which could make good resource states for the generation of non-Gaussian states via postselection, particularly in situations where mode tunability is desired, e.g., to compensate for loss.

Future work could investigate the effects of time ordering on the JSA [44], suppression of modes within the crystal using

photonic stop bands [45], and possible applications in other areas of research such as multiparameter quantum metrology [7] and multichannel quantum imaging [8]. We expect that exploring new quantum states of light, encoded in new degrees of freedom, such as those proposed here, will be a key element in developing future quantum technologies.

The JUPYTER notebook used to generate the results in this paper can be found in [46].

ACKNOWLEDGMENTS

A.M.B. thanks Austin Lund, Olivier Pfister, and Alessandro Fedrizzi for valuable discussions. Research at Perimeter Institute was supported in part by the Government of Canada through the Department of Innovation, Science and Economic Development Canada and by the Province of Ontario through the Ministry of Colleges and Universities. We acknowledge support from the Natural Sciences and Engineering Research Council of Canada (Grant No. RGPIN-2016-04135).

APPENDIX A: REVIEW OF SQUEEZED STATES

Here we briefly review single-mode, two-mode, and multimode squeezed states. A squeezed state prepared in a single mode \hat{a}_0 can be written as [47]

$$|\text{SMSV}\rangle = e^{\beta_{00}\hat{a}_0^\dagger\hat{a}_0/2 - \text{H.c.}} |\text{vac}\rangle, \quad (\text{A1})$$

where β_{00} is the complex single-mode squeezing parameter. If we define the uncertainty of an operator \hat{A} by $(\Delta A)^2 = \langle \text{SMSV} | (\hat{A} - \langle A \rangle)^2 | \text{SMSV} \rangle$, the single-mode squeezed state has the property that it minimizes the uncertainty relation below the quantum noise limit. This is taken advantage of in quantum sensing experiments, where one decreases the phase uncertainty to measure changes in distance beyond the quantum noise limit [48,49].

A two-mode squeezed state prepared in modes \hat{a}_0 and \hat{a}_1 can be written as [47]

$$|\text{TMSV}\rangle = e^{\beta_{01}\hat{a}_0^\dagger\hat{a}_1^\dagger - \text{H.c.}} |\text{vac}\rangle, \quad (\text{A2})$$

where β_{01} is the complex two-mode squeezing parameter. If one considers the effect that the squeezing operator has on the variance of the sum and difference of each mode's conjugate variables, one finds a squeezing effect similar to that for the single-mode state. For the two operators \hat{A} and \hat{B} , the two-mode squeezed state minimizes the uncertainty relation between the conjugate variables $\hat{A} - \hat{B}$ and $\hat{A} + \hat{B}$ below the quantum noise limit. The reduction in noise between $\hat{A} - \hat{B}$ generates a high degree of correlation, and in the limit when $|\beta_{01}| \rightarrow \infty$, two-mode squeezed states are the continuous-variable extension of maximally entangled Bell states [50]. The entanglement properties of two-mode squeezed state can be used for various quantum information protocols such as quantum teleportation and quantum cryptography [1,2].

The squeezed states above can be generalized to N -partite entangled states as

$$|\text{MMSV}\rangle = \exp\left(\frac{1}{2} \sum_{n,m} \beta_{nm} \hat{a}_n^\dagger \hat{a}_m^\dagger - \text{H.c.}\right) |\text{vac}\rangle, \quad (\text{A3})$$

where the double sum in the exponential ranges from $n, m = -N, -N+1, \dots, 0, \dots, N-1, N$ and due to symmetry we take $\beta_{nm} = \beta_{mn}$. These multimode squeezed states can be used to generalize various quantum information protocols [51,52].

APPENDIX B: SPONTANEOUS PARAMETRIC DOWN-CONVERSION

In this Appendix we review the nonlinear-optical process known as spontaneous parametric down-conversion (SPDC). In a SPDC process the input photons, typically called pump photons, are each down-converted into two daughter photons, called the signal and idler. The signal and idler photons satisfy energy and momentum conservation with the pump photon given by

$$\omega_p = \omega_s + \omega_i, \quad k_p(\omega_p) = k_s(\omega_s) + k_i(\omega_i), \quad (\text{B1})$$

where ω_j and $k_j(\omega_j)$ are the frequency and wave vectors. The three fields of interest are labeled by $J = p, s, i$, denoting the pump, signal, and idler, respectively. A detailed derivation of SPDC was given in [53], which we follow.

For a type II down-conversion process [in the rotating-wave approximation, assuming the material is in an effective one-dimensional (1D) structure where the field does not vary in the orthogonal direction of area A (for a review of effective 1D structures see [53–57]), with a nonlinear coefficient $\chi^{(2)}(z)$ that varies along the longitudinal direction z] the nonlinear Hamiltonian in the interaction picture is

$$\begin{aligned} \hat{H}_I(t) = & -\hbar \int_0^\infty d\omega_p d\omega_i d\omega_s \hat{c}_V(\omega_p) \hat{a}_V^\dagger(\omega_i) \hat{a}_H^\dagger(\omega_s) \\ & \times e^{i(\omega_s + \omega_i - \omega_p)t} 2L \sqrt{\frac{\hbar \omega_p \omega_i \omega_s}{(4\pi)^3 \epsilon_0 A c^3 n_p(\omega_p) n_s(\omega_s) n_i(\omega_i)}} \\ & \times \frac{1}{L} \int_{-L/2}^{L/2} dz \chi^{(2)}(z) e^{i(k_p(\omega_p) - k_i(\omega_i) - k_s(\omega_s))z} + \text{H.c.} \end{aligned} \quad (\text{B2})$$

For nonlinear materials we will be considering, $\chi^{(2)}(z)$ is constant over a specified domain length and given by $\chi^{(2)}(z) = \pm \chi^{(2)}$. We find it useful to define

$$g(z) = \frac{\chi^{(2)}(z)}{\chi^{(2)}} \quad (\text{B3})$$

to be the scaled nonlinearity function which has two values given by $g(z) = \pm 1$. If we take the initial ket $|\psi(-\infty)\rangle$ to be a coherent state in the pump mode and the signal and idler vacuum, then in the undepleted pump approximation (where we assume the pump light is unchanged with the removal of a photon) we can make the substitution

$$\hat{c}_V(\omega_p) \rightarrow \sqrt{|\alpha_p|} \alpha(\omega_p), \quad (\text{B4})$$

where $\alpha(\omega_p)$ is the normalized frequency distribution of the pump laser, which satisfies

$$\int |\alpha(\omega)|^2 d\omega = 1, \quad (\text{B5})$$

and $|\alpha_p|^2$ is the number of photons in the pump. Then the Hamiltonian is given by

$$\hat{H}_I(t) = -\hbar \int_0^\infty d\omega_p d\omega_i d\omega_s \mathcal{A}(\omega_i, \omega_s, \omega_p) \alpha(\omega_p) \Phi(\omega_s, \omega_i, \omega_p) \hat{a}_V^\dagger(\omega_i) \hat{a}_H^\dagger(\omega_s) e^{i(\omega_s + \omega_i - \omega_p)t} + \text{H.c.}, \quad (\text{B6})$$

where we set

$$\mathcal{A}(\omega_s, \omega_i, \omega_p) = 2L\chi^{(2)} \sqrt{\frac{\sqrt{|\alpha_p|} \hbar \omega_p \omega_i \omega_s}{(4\pi)^3 \epsilon_0 A c^3 n_p(\omega_p) n_s(\omega_s) n_i(\omega_i)}}, \quad (\text{B7})$$

define

$$\Phi(\Delta k(\omega_i, \omega_s, \omega_p)) = \frac{1}{L} \int_{-L/2}^{L/2} dz g(z) e^{i\Delta k(\omega_p, \omega_s, \omega_i)z} \quad (\text{B8})$$

to be the phase-matching function, and set $\Delta k(\omega_p, \omega_s, \omega_i) = k_p(\omega_p) - k_i(\omega_i) - k_s(\omega_s)$ to be the phase mismatch.

In the interaction picture the states evolves according to interaction Hamiltonian given by [58]

$$i\hbar \frac{d|\psi(t)\rangle}{dt} = \hat{H}_I(t) |\psi(t)\rangle, \quad (\text{B9})$$

$$|\psi\rangle = \exp\left(i \int d\omega_s d\omega_i \mathcal{A}(\omega_i, \omega_s) \alpha(\omega_i + \omega_s) \Phi(\Delta k(\omega_i, \omega_s)) \hat{a}_H^\dagger(\omega_i) \hat{a}_V^\dagger(\omega_s) + \text{H.c.}\right) |\text{vac}\rangle, \quad (\text{B11})$$

where we made the simplifications $\mathcal{A}(\omega_s, \omega_i, \omega_i + \omega_s) \rightarrow \mathcal{A}(\omega_s, \omega_i)$ and $\Phi(\Delta k(\omega_i, \omega_s, \omega_i + \omega_s)) \rightarrow \Phi(\Delta k(\omega_i, \omega_s))$ with

$$\Delta k(\omega_i, \omega_s) = k_p(\omega_i + \omega_s) - k_i(\omega_i) - k_s(\omega_s) \quad (\text{B12})$$

the phase mismatch and $k_J(\omega_J) = \omega_J n_J(\omega_J)/c$. Finally, for the frequency range of interest, to a good approximation we can evaluate the frequency-dependent term $\mathcal{A}(\omega_s, \omega_i) \approx \mathcal{A}(\Omega_s, \Omega_i) = \mathcal{A}$, where Ω_s and Ω_i are the center frequencies of the signal and idler.

To push the equations further, we expand the phase mismatch Δk to first order around the center frequencies $\Omega_s, \Omega_i, \Omega_p = \Omega_s + \Omega_i$ such that

$$\Delta k(\omega_i, \omega_s) = \Delta k_0 + k'_p(\omega_p - \Omega_p) - k'_i(\omega_i - \Omega_i) - k'_s(\omega_s - \Omega_s), \quad (\text{B13})$$

where we set $\Delta k_0 = k_p(\Omega_s + \Omega_i) - k_i(\Omega_i) - k_s(\Omega_s)$, the first-order derivatives are $k'_j = \partial k_j(\omega_j)/\partial \omega_j|_{\omega_j=\Omega_j}$, and energy conservation ensures that $\omega_p = \omega_i + \omega_s$ and $\Omega_p = \Omega_i + \Omega_s$. Next we work in the symmetric group-velocity matching regime such that $k'_p = (k'_s + k'_i)/2$. Then with these choices we are left with

$$\Delta k(\omega_i, \omega_s) = \Delta k_0 + \frac{k'_s - k'_i}{2} [(\omega_i - \Omega_i) - (\omega_s - \Omega_s)]. \quad (\text{B14})$$

We note that $\Delta k(\omega_i, \omega_s)$ is now a function of the variable $\omega_i - \omega_s$ so we take $\Delta k(\omega_i, \omega_s) \rightarrow \Delta k(\omega_i - \omega_s)$ and therefore $\Phi(\Delta k(\omega_i, \omega_s)) \rightarrow \Phi(\omega_i - \omega_s)$, which for typical

which has a formal solution of

$$|\psi(\infty)\rangle = \mathcal{T} \left[\exp\left(\frac{-i}{\hbar} \int_{-\infty}^{\infty} dt \hat{H}_I(t)\right) \right] |\psi(-\infty)\rangle, \quad (\text{B10})$$

where \mathcal{T} is the time-ordering operator and $|\psi(\infty)\rangle$ is the final state. Since the interaction Hamiltonian does not commute with itself at different times, we cannot in general drop the time-ordering operator. It was shown in [44] that the time ordering leads to nontrivial effects but only in the high-pump-power regime. For this work, we will assume low pump powers and not worry about these time-ordering effects, i.e., we drop the time-ordering operator. Then integrating the interaction Hamiltonian with respect to t introduces an energy-conserving delta function $\delta(\omega_s + \omega_i - \omega_p)$ which we use to evaluate the ω_p integral. Then the state is given by

phase-matching functions will be peaked along the diagonal. Calculating the square integral of $\Phi(\omega)$, we find it is not yet normalized and set its value to be \mathcal{N}^2 for some \mathcal{N} , then

$$\int d\omega |\Phi(\omega)|^2 = \mathcal{N}^2. \quad (\text{B15})$$

To normalize $\Phi(\omega)$ we define

$$\phi(\omega) = \frac{2}{\mathcal{N}} \Phi(\omega). \quad (\text{B16})$$

Then the squeezed state is given by

$$|\psi\rangle = \exp\left(i\gamma \int d\omega_s d\omega_i f(\omega_s, \omega_i) \hat{a}_H^\dagger(\omega_i) \hat{a}_V^\dagger(\omega_s) + \text{H.c.}\right) \times |\text{vac}\rangle, \quad (\text{B17})$$

where we defined the squeezing parameter γ to be $\gamma = \mathcal{A}\mathcal{N}/2$ and defined the JSA as

$$f(\omega_s, \omega_i) = \alpha(\omega_i + \omega_s) \phi(\omega_i - \omega_s), \quad (\text{B18})$$

which due to the normalization in Eqs. (B5) and (B16) satisfies the normalization

$$\int d\omega_s d\omega_i |f(\omega_s, \omega_i)|^2 = 1. \quad (\text{B19})$$

APPENDIX C: BIAS IN THE PMF

For a crystal of length L the approximate phase-matching function is given by

$$\Phi_a(\Delta k) = \frac{1}{L} \int_{-L/2}^{L/2} dz g_a(z) e^{i\Delta k z}, \quad (\text{C1})$$

where $g_a(z)$ is the approximate nonlinearity function specified by the poling algorithm and is either ± 1 . The phase-matching function can be written as a coherent sum by expanding the integral over z into each domain by

$$\Phi_a(\Delta k) = \frac{1}{L} \sum_{n=0}^{n=N} g_n \int_{-L/2+nl_c}^{-L/2+(n+1)l_c} e^{i\Delta k z} dz, \quad (\text{C2})$$

where l_c is the coherence length, $Nl_c = L$, and $g_n \equiv g_a[-\frac{L}{2} + nl_c \leq z \leq -\frac{L}{2} + (n+1)l_c]$ is the nonlinearity within each domain. Then evaluating the integral and simplifying the approximate phase-matching function, we obtain

$$\Phi_a(\Delta k) = \frac{l_c}{L} \text{sinc}\left(\frac{\Delta k l_c}{2}\right) e^{i\Delta k l_c/2} e^{-i\Delta k L/2} \sum_{n=0}^{n=N} g_n e^{i\Delta k l_c n}. \quad (\text{C3})$$

Since the algorithm we are using to determine g_n is only for real phase-matching functions we know the imaginary part will sum to zero and the nonzero contribution is only from the real part, which is given by

$$\Re \Phi_a(\Delta k) = \frac{l_c}{L} \frac{\sin\left(\frac{\Delta k l_c}{2}\right)}{\left(\frac{\Delta k l_c}{2}\right)} \sum_{n=0}^{n=N} g_n \cos\left(\frac{\Delta k l_c}{2}(2n+1-N)\right), \quad (\text{C4})$$

which is manifestly symmetric about $\Delta k = 0$. However, the phase-matching function we are designing has peaks at $\Delta k = \Delta k_0 \pm m\delta k$, which are centered at Δk_0 , ensuring the nonlinear generation is phase matched. Evaluating the approximate phase-matching function in this vicinity leads to a $1/(\Delta k_0 \pm m\delta k)$ dependence which is no longer symmetric

and leads to a bias on the left and right sides of Δk_0 shown in Fig. 1.

Although the phase-matching function bias for large or smaller values of Δk leads to less accurate PMFs, by decreasing the coherence length the affect of the bias is lessened and the PMF is better approximated. We can understand why this necessarily follows in two ways. First we decrease the coherence length the sinc function prefactor in Eq. (C4) becomes more broad and is therefore constant for larger values of Δk , minimizing the bias. Second, by decreasing the coherence length we are increasing the ‘‘resolution’’ of our tracking algorithm, which increases the accuracy of the approximated PMF. To further increase the accuracy of the generated PMFs we can move to subcoherence domain engineering, which was discussed in detail by Graffitti *et al.* in [40].

APPENDIX D: DESIGN CONSIDERATIONS

Quasi-phase-matched periodically poled crystals are known to generate amplitudes reduced by a factor of $2/\pi$ when compared with their phase-matched counterparts [37]. For example, if the unnormalized phase-matching function for a phase-matched crystal of length L is $\Phi(\Delta k) = \frac{1}{L} \int_{-L/2}^{L/2} e^{-i\Delta k z} dz = \text{sinc}(\Delta k L/2)$, then for a periodically poled crystal it is $\Phi(\Delta k) \approx (2/\pi) \text{sinc}(\Delta k L/2)$. This is due to the interference behind the quasi-phase-matching effect. The phase-matching function is at its maximum value of $2/\pi$ at the phase-matching condition ($\Delta k = 0$). The amplitude along the longitudinal direction z is $2z/L\pi$, which defines the maximum slope for the amplitude inside the crystal.

We can use the maximum slope restriction to put bounds on the coefficients c_n that scale each Gaussian peak in the target PMFs by making sure that the gradient of the amplitude function satisfies

$$\frac{d}{dz} A_t(z, \Delta k_0) \leq \frac{d}{dz} \left(\frac{2z}{\pi L} \right) = \frac{2}{\pi L}. \quad (\text{D1})$$

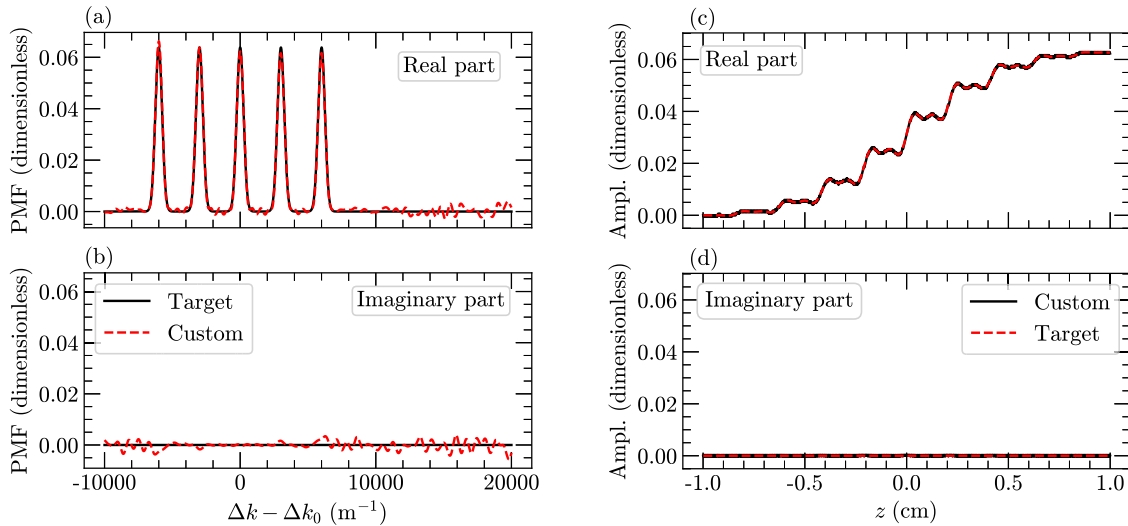


FIG. 4. (a) Real part and (b) imaginary part of the five-peak target phase-matching function as defined in Eq. (17) (with $c_m = \sqrt{2}/\sqrt{\pi}L5\sigma_k$, $\sigma_k = 2.5/L$, and $\delta k = 24\sigma_k$) and (c) real part and (d) imaginary part of the corresponding amplitude function. We took $\sigma_k = 2.5/L$ to ensure that the target nonlinearity profile fits within the length of the crystal. The custom-poled crystal has $N = 1073$ domains of width $w = 18.63 \mu\text{m}$. The domain width was chosen to match the phase-matching conditions of type-II KTP in the symmetric group-velocity-matched regime.

The amplitude of the PMF for a given Δk_0 throughout the crystal is given by

$$A_t(z, \Delta k_0) = \frac{1}{L} \int_{-L/2}^z dz' g_t(z') e^{i\Delta k_0 z'}. \quad (\text{D2})$$

Figures 4(c) and 4(d) shows an example amplitude function for the 5-peak PMF in Figs. 4(a) and 4(b). Then the target nonlinearity function $g_t(z)$ can be found by inverting Eq. (16):

$$g_t(z) = \frac{L}{2\pi} \int_{-\infty}^{\infty} d(\Delta k) \Phi_t(\Delta k) e^{-i\Delta k z}. \quad (\text{D3})$$

We now pick a specific form for the target PMF $\Phi_t(\Delta k)$ with $N_G = 2N + 1$ Gaussian amplitudes,

$$\Phi_t(\Delta k) = \sum_{m=-N}^N c_m e^{-(\Delta k - \Delta k_0 - m\delta k)^2 / 8\sigma_k^2}, \quad (\text{D4})$$

and insert it into (D3) to give

$$g_t(z) \approx \frac{2L\sigma_k}{\sqrt{2\pi}} e^{-2z^2\sigma_k^2} e^{-i\Delta k_0 z} \left(c_0 + 2 \sum_{m=1}^N c_m \cos(m\delta k z) \right), \quad (\text{D5})$$

where we used the approximation that the amplitudes of the PMF are symmetric ($c_m = c_{-m}$). Now inserting (D5) into (D2) and taking the derivative with respect to z , we find that the coefficients must satisfy

$$\frac{2\sigma_k}{\sqrt{2\pi}} e^{-2z^2\sigma_k^2/2} \left(c_0 + 2 \sum_{m=1}^N c_m \cos(m\delta k z) \right) \leq \frac{2}{\pi L}. \quad (\text{D6})$$

If the inequality holds for $z = 0$, it holds for all z . Then taking the inequality at $z = 0$, the amplitude coefficients c_m must satisfy

$$c_0 + 2 \sum_{m=1}^N c_m \leq \sqrt{\frac{2}{\pi}} \frac{1}{L\sigma_k}. \quad (\text{D7})$$

If we ensure that the prefactor coefficients satisfy the above inequality, we guarantee that the target PMF amplitude can always be tracked by changing the domains of the crystal. More sophisticated treatments can be made to determine the optimal choice of constants c_m by considering different choices of z but as a first consideration we stop with the inequality in Eq. (D7).

-
- [1] G. J. Milburn and S. L. Braunstein, Quantum teleportation with squeezed vacuum states, *Phys. Rev. A* **60**, 937 (1999).
- [2] M. Hillery, Quantum cryptography with squeezed states, *Phys. Rev. A* **61**, 022309 (2000).
- [3] J. M. Arrazola, V. Bergholm, K. Brádler, T. R. Bromley, M. J. Collins, I. Dhand, A. Fumagalli, T. Gerrits, A. Goussev, L. G. Helt *et al.*, Quantum circuits with many photons on a programmable nanophotonic chip, *Nature (London)* **591**, 54 (2021).
- [4] R. S. Bennink, S. J. Bentley, R. W. Boyd, and J. C. Howell, Quantum and Classical Coincidence Imaging, *Phys. Rev. Lett.* **92**, 033601 (2004).
- [5] R. Schnabel, N. Mavalvala, D. E. McClelland, and P. K. Lam, Quantum metrology for gravitational wave astronomy, *Nat. Commun.* **1**, 121 (2010).
- [6] A. I. Lvovsky, in *Photonics*, edited by D. Andrews (Wiley, Chichester, 2015), pp. 121–164.
- [7] M. Gessner, L. Pezzè, and A. Smerzi, Sensitivity Bounds for Multiparameter Quantum Metrology, *Phys. Rev. Lett.* **121**, 130503 (2018).
- [8] I. V. Sokolov and M. I. Kolobov, Squeezed-light source for superresolving microscopy, *Opt. Lett.* **29**, 703 (2004).
- [9] Y. Lian, C. Xie, and K. Peng, Continuous variable multipartite entanglement and optical implementations of quantum communication networks, *New J. Phys.* **9**, 314 (2007).
- [10] N. Fabre, G. Maltese, F. Appas, S. Felicetti, A. Ketterer, A. Keller, T. Coudreau, F. Baboux, M. I. Amanti, S. Ducci, and P. Milman, Generation of a time-frequency grid state with integrated biphoton frequency combs, *Phys. Rev. A* **102**, 012607 (2020).
- [11] H. P. Yuen, Two-photon coherent states of the radiation field, *Phys. Rev. A* **13**, 2226 (1976).
- [12] G. Yeoman and S. M. Barnett, Two-mode squeezed gaussons, *J. Mod. Opt.* **40**, 1497 (1993).
- [13] P. van Loock and S. L. Braunstein, Multipartite Entanglement for Continuous Variables: A Quantum Teleportation Network, *Phys. Rev. Lett.* **84**, 3482 (2000).
- [14] M. S. Elezov, M. L. Scherbatenko, D. V. Sych, and G. N. Goltsman, Active and passive phase stabilization for the all-fiber Michelson interferometer, *J. Phys.: Conf. Ser.* **1124**, 051014 (2018).
- [15] O. Pfister, S. Feng, G. Jennings, R. Pooser, and D. Xie, Multipartite continuous-variable entanglement from concurrent nonlinearities, *Phys. Rev. A* **70**, 020302(R) (2004).
- [16] N. C. Menicucci, S. T. Flammia, H. Zaidi, and O. Pfister, Ultracompact generation of continuous-variable cluster states, *Phys. Rev. A* **76**, 010302(R) (2007).
- [17] R. N. Alexander, P. Wang, N. Sridhar, M. Chen, O. Pfister, and N. C. Menicucci, One-way quantum computing with arbitrarily large time-frequency continuous-variable cluster states from a single optical parametric oscillator, *Phys. Rev. A* **94**, 032327 (2016).
- [18] X. Zhu, C.-H. Chang, C. González-Arciniegas, A. Pe'er, J. Higgins, and O. Pfister, Hypercubic cluster states in the phase-modulated quantum optical frequency comb, *Optica* **8**, 281 (2021).
- [19] V. Ansari, J. M. Donohue, B. Brecht, and C. Silberhorn, Tailoring nonlinear processes for quantum optics with pulsed temporal-mode encodings, *Optica* **5**, 534 (2018).
- [20] C. L. Morrison, F. Graffitti, P. Barrow, A. Pickston, J. Ho, and A. Fedrizzi, Frequency-bin entanglement from domain-engineered down-conversion, *APL Photon.* **7**, 066102 (2022).
- [21] S. Lloyd, Programming pulse driven quantum computers, *Science* **261**, 1569 (1993).
- [22] C. Couteau, Spontaneous parametric down-conversion, *Contemp. Phys.* **59**, 291 (2018).
- [23] A. M. Weiner, Ultrafast optical pulse shaping: A tutorial review, *Opt. Commun.* **284**, 3669 (2011).

- [24] C. Froehly, B. Colombeau, and M. Vampouille, II shaping and analysis of picosecond light pulses, *Prog. Opt.* **20**, 63 (1983).
- [25] A. Monmayrant, S. Weber, and B. Chatel, A newcomer's guide to ultrashort pulse shaping and characterization, *J. Phys. B* **43**, 103001 (2010).
- [26] N. Quesada and A. M. Brańczyk, Gaussian functions are optimal for waveguided nonlinear-quantum-optical processes, *Phys. Rev. A* **98**, 043813 (2018).
- [27] R. W. Boyd, *Nonlinear Optics* (Academic Press, New York, 2019).
- [28] A. Zukauskas, G. Strömquist, V. Pasiskevicius, F. Laurell, M. Fokine, and C. Canalias, Fabrication of submicrometer quasi-phase-matched devices in KTP and RKTP, *Opt. Mater. Express* **1**, 1319 (2011).
- [29] M. M. Fejer, G. A. Magel, D. H. Jundt, and R. L. Byer, Quasi-phase-matched second harmonic generation: tuning and tolerances, *IEEE J. Quantum Electron.* **28**, 2631 (1992).
- [30] G. Imeshev, M. A. Arbore, M. M. Fejer, A. Galvanauskas, M. Fermann, and D. Harter, Ultrashort-pulse second-harmonic generation with longitudinally nonuniform quasi-phase-matching gratings: Pulse compression and shaping, *J. Opt. Soc. Am. B* **17**, 304 (2000).
- [31] M. A. Arbore, A. Galvanauskas, D. Harter, M. H. Chou, and M. M. Fejer, Engineerable compression of ultrashort pulses by use of second-harmonic generation in chirped-period-poled lithium niobate, *Opt. Lett.* **22**, 1341 (1997).
- [32] P. B. Dixon, J. H. Shapiro, and F. N. C. Wong, Spectral engineering by Gaussian phase-matching for quantum photonics, *Opt. Express* **21**, 5879 (2013).
- [33] C. Chen, C. Bo, M. Y. Niu, F. Xu, Z. Zhang, J. H. Shapiro, and F. N. C. Wong, Efficient generation and characterization of spectrally factorable biphotons, *Opt. Express* **25**, 7300 (2017).
- [34] C. Chen, J. E. Heyes, K.-H. Hong, M. Y. Niu, A. E. Lita, T. Gerrits, S. W. Nam, J. H. Shapiro, and F. N. C. Wong, Indistinguishable single-mode photons from spectrally engineered biphotons, *Opt. Express* **27**, 11626 (2019).
- [35] C. Cui, R. Arian, S. Guha, N. Peyghambarian, Q. Zhuang, and Z. Zhang, Wave-Function Engineering for Spectrally Uncorrelated Biphotons in the Telecommunication Band Based on a Machine-Learning Framework, *Phys. Rev. Appl.* **12**, 034059 (2019).
- [36] A. M. Brańczyk, A. Fedrizzi, T. M. Stace, T. C. Ralph, and A. G. White, Engineered optical nonlinearity for quantum light sources, *Opt. Express* **19**, 55 (2011).
- [37] J. L. Tambasco, A. Boes, L. G. Helt, M. J. Steel, and A. Mitchell, Domain engineering algorithm for practical and effective photon sources, *Opt. Express* **24**, 19616 (2016).
- [38] A. Dosseva, E. Cincio, and A. M. Brańczyk, Shaping the joint spectrum of down-converted photons through optimized custom poling, *Phys. Rev. A* **93**, 013801 (2016).
- [39] F. Graffitti, P. Barrow, M. Proietti, D. Kundys, and A. Fedrizzi, Independent high-purity photons created in domain-engineered crystals, *Optica* **5**, 514 (2018).
- [40] F. Graffitti, D. Kundys, D. T. Reid, A. M. Brańczyk, and A. Fedrizzi, Pure down-conversion photons through sub-coherence-length domain engineering, *Quantum Sci. Technol.* **2**, 035001 (2017).
- [41] A. Pickston, F. Graffitti, P. Barrow, C. L. Morrison, J. Ho, A. M. Brańczyk, and A. Fedrizzi, Optimised domain-engineered crystals for pure telecom photon sources, *Opt. Express* **29**, 6991 (2021).
- [42] F. Graffitti, J. Kelly-Massicotte, A. Fedrizzi, and A. M. Brańczyk, Design considerations for high-purity heralded single-photon sources, *Phys. Rev. A* **98**, 053811 (2018).
- [43] M. Yamada, N. Nada, M. Saitoh, and K. Watanabe, First-order quasi-phase matched LiNbO₃ waveguide periodically poled by applying an external field for efficient blue second-harmonic generation, *Appl. Phys. Lett.* **62**, 435 (1993).
- [44] N. Quesada and J. E. Sipe, Why you should not use the electric field to quantize in nonlinear optics, *Opt. Lett.* **42**, 3443 (2017).
- [45] L. G. Helt, A. M. Brańczyk, M. Liscidini, and M. J. Steel, Parasitic Photon-Pair Suppression via Photonic Stop-Band Engineering, *Phys. Rev. Lett.* **118**, 073603 (2017).
- [46] <https://github.com/abrancyk/custom-poling>
- [47] M. O. Scully and M. S. Zubairy, *Quantum Optics* (Cambridge University Press, Cambridge, 1997).
- [48] B. J. Lawrie, P. D. Lett, A. M. Marino, and R. C. Pooser, Quantum sensing with squeezed light, *ACS Photon.* **6**, 1307 (2019).
- [49] J. Aasi, J. Abadie, B. P. Abbott, R. Abbott, T. D. Abbott, M. R. Abernathy, C. Adams, T. Adams, P. Addesso, R. X. Adhikari *et al.*, Enhanced sensitivity of the LIGO gravitational wave detector by using squeezed states of light, *Nat. Photon.* **7**, 613 (2013).
- [50] X.-B. Wang, T. Hiroshima, A. Tomita, and M. Hayashi, Quantum information with gaussian states, *Phys. Rep.* **448**, 1 (2007).
- [51] S. Armstrong, J.-F. Morizur, J. Janousek, B. Hage, N. Treps, P. K. Lam, and H.-A. Bachor, Programmable multimode quantum networks, *Nat. Commun.* **3**, 1026 (2012).
- [52] M. Epping, H. Kampermann, C. Macchiavello, and D. Bruß, Multi-partite entanglement can speed up quantum key distribution in networks, *New J. Phys.* **19**, 093012 (2017).
- [53] Z. Yang, M. Liscidini, and J. E. Sipe, Spontaneous parametric down-conversion in waveguides: A backward Heisenberg picture approach, *Phys. Rev. A* **77**, 033808 (2008).
- [54] N. Quesada, L. G. Helt, M. Menotti, M. Liscidini, and J. E. Sipe, Beyond photon pairs—nonlinear quantum photonics in the high-gain regime: A tutorial, *Adv. Opt. Photon.* **14**, 291 (2022).
- [55] J. E. Sipe, N. A. R. Bhat, P. Chak, and S. Pereira, Effective field theory for the nonlinear optical properties of photonic crystals, *Phys. Rev. E* **69**, 016604 (2004).
- [56] K. J. Blow, R. Loudon, S. J. D. Phoenix, and T. J. Shepherd, Continuum fields in quantum optics, *Phys. Rev. A* **42**, 4102 (1990).
- [57] J. N. Q. Mejia, *Very Nonlinear Quantum Optics* (University of Toronto Press, Toronto, 2015).
- [58] R. Shankar, *Principles of Quantum Mechanics* (Springer Science + Business Media, New York, 2012).